Published 28 February 2025 by the University of KwaZulu-Natal https://journals.ukzn.ac.za/index.php/JICBE
© Creative Commons With Attribution (CC-BY)

Journal of Inclusive cities and Built environment. Vol. 3 Issue 5

How to cite: B. Kassum, M. Nkoom, et al., 2025. Sustainable Alternatives: The Role of Natural Sponge Fibre in Enhancing Concrete Properties and limiting the impacts associated with climate change. *Journal of Inclusive cities and Built environment*. Vol. 3 Issue 5, Pg 93-113.

SUSTAINABLE ALTERNATIVES: THE ROLE OF NATURAL SPONGE FIBRE IN ENHANCING CONCRETE PROPERTIES AND LIMITING THE IMPACTS ASSOCIATED WITH CLIMATE CHANGE

By B. Kassum, M. Nkoom, C.N.A. Acquay and A.O. Antwi

Published 31 July 2025

ABSTRACT

The use of polymer and steel fibres to alleviate the brittleness of mass concrete has been extensively researched. However, increased awareness of the environmental hazards associated with the gases emitted into the atmosphere such as carbon dioxide during production has prompted efforts to reduce global temperatures to below 2°C. Natural sponge fibre (NSF)- reinforced concrete is being produced as an eco-friendly substitute for polymer and steel fibrereinforced concrete. Thus, the study aims to assess the effects of untreated (NonC) and sodium hydroxide (N)treated NSF on the microstructure, diffusion, and mechanical properties of NSF-reinforced concrete (NSFRC), as well as their environmental benefits. A mass concrete mixture was prepared as a control (CTRL) and compared with mixtures containing untreated and N-treated NSF at various fibre weight fractions of 0.00%, 0.75%, 1.00%, and 1.25%. Beams were cast for four-point bending tests. Prisms and core discs extracted from the tested beams were used to examine axial compressive strength and durability after exposure. Scanning electron microscopy (SEM) was employed to analysis the surface morphology of the NSF and the fractured concrete. Test results of N-treated NSFRC beams showed a more robust flexural load-carrying capacity, demonstrating strain hardening in the rising portion of the curves after the first crack and enhanced durability compared to all the specimens. As anticipated, the plain concrete specimens failed without warning signs at the cracking stage. The strong fibre bond resulted in minimal fibre inelastic buckling, minor matrix cracks, high energy absorption, and axial compressive strength. N-treated NSFRC prisms demonstrated these qualities, and the splitting of specimens as a mode of failure was reduced. Generally, the treatment efficacy and the fibre abridgement proved to be responsible for the results. Micrograph analysis confirms that sodium hydroxide-treated NSFRC has potential as a sustainable, eco-friendly, and cost-effective alternative to conventional fibre-reinforced concrete in construction.

KEY WORDS Sustainable material, Natural sponge fibre, Ecologically friendly, Strength

Braimah Kassum, (PhD): Department of Built Environment, University of Environment and Sustainable Development, Somanya, Ghana, School of Engineering, Department of Civil Engineering, University of KwaZulu-Natal, Durban, 4041, South Africa. Email: kbraimah@uesd.edu.gh

Matthew Nkoom, (PhD): Department of Built Environment, University of Environment and Sustainable Development, Somanya, Ghana. Email: mnkoom@uesd.edu.gh Cynthia Naa Adoley Acquaye, (MSc): Department of Built Environment, University of Environment and Sustainable Development, Somanya, Ghana. Email: cnaacquaye@uesd.edu.gh

Adwoa Oforiwa Antwi3, (PhD): Department of Built Environment, University of Environment and Sustainable Development, Somanya, Ghana. Email: aoantwi@uesd.ed.gh

1. INTRODUCTION

Cement, water, aggregate (such as sand or gravel), and occasionally additives are the ingredients of conventional concrete, a building material. From little home foundations to massive commercial structures and infrastructure projects, it is extensively utilized in a wide range of construction projects. Due to its adaptability, conventional concrete has been a vital component of construction for millennia [Maturix, 2023]. The properties of the concrete mixture and the surrounding environment contribute to unfavourable cracking under flexure, resulting in a reduction in long-term strength [American Concrete Institute, 2020]._

In structural applications, fibre-reinforced composites have become increasingly popular for addressing the shortcomings of conventional concretes, particularly in terms of strength and durability. This development has led to the invention of steel and polymer fibre-reinforced concrete [Xie et al., 2020, 2021; Tans et al., 2022]. These conventional reinforcements are incorporated within the structure to withstand applied tensile and shear stresses [Xie et al., 2021]. Several researchers have demonstrated that incorporating fibres (steel and synthetic polymers) into cementitious materials enhances their mechanical and physical properties [Ige, 2016; Wei and Gencturk, 2018; Hasan et al., 2021].

When compared to natural fibre concrete, polymer and steel concrete have issues with greenhouse gas emissions and environmental sustainability. Carbon emissions are a significant concern, particularly in the production of steel and the polymers used in concrete. Specifically, energy-intensive chemical reactions that are frequently produced from fossil fuels are required to make steel and polymers, resulting in considerable emissions of carbon dioxide into the environment [Salami et al., 2024]. In addition to enhancing other qualities, scientists are constantly working to improve concrete to lessen the adverse environmental effects of conventional fibre concretes.

Therefore, utilizing natural fibres is a step in the direction of a more sustainable strategy. Natural fibres are classified into plant-based and animal-based fibres. The plant fibres consist of cellulose, hemicellulose, lignin, and pectin [Mohanty et al., 2001; Kabir et al., 2012], with cellulose and lignin being the major components. Structurally, cellulose is a semi-crystalline, hydrophilic polysaccharide composed of straight chains of anhydroglucose units containing hydroxyl groups found in plants. Hemicellulose is a branched, hydrolysable polysaccharide that interacts with cellulose [Li et al., 2014; Zhang et al., 2013, 2022]. For lignin, it acts as a binding matrix, securing cellulose and hemicellulose within a pectin network. Furthermore, these fibres are sourced from specific plant parts such as bast fibres (stem): Jute, hemp, flax, and kenaf. The other sources are leaves, seeds, fruit, stalks, and grass/cane. Natural sponge fibres (see Figure 1) represent a distinct subcategory within the bast fibres.

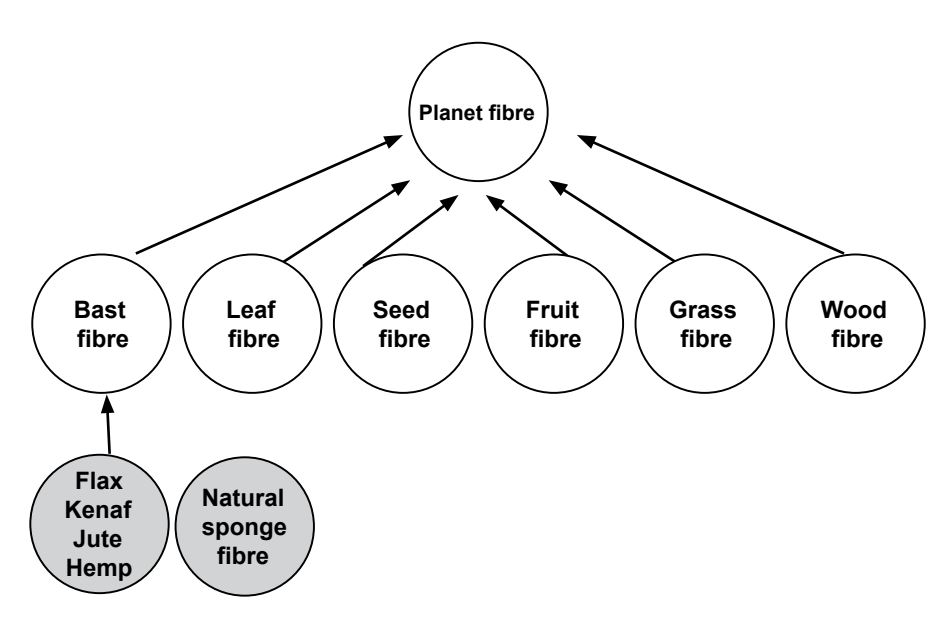


Figure 1. Classification of plant fibres (introduced – natural sponge fibre)

Natural fibres are used in a variety of ways, such as building materials, particle boards, insulation, etc. Natural fibres can improve the mechanical and durability qualities of cementitious composites and are a sustainable alternative to conventional fibres. When compared to composites made from traditional fibres, these natural, plant-based fibre composites offer several benefits. In addition, natural fibres are biodegradable, non-toxic, widely accessible, non-abrasive, lightweight, reasonably priced, and have a high specific strength [Fahim et al., 2012]. They also show outstanding resistance to corrosion and fatigue [Abdalla et al., 2023]. Due to their advantages, natural fibres are ideal for producing environmentally friendly concrete that can be scaled up to meet the current demand for sustainable structures [Thomas et al., 2021, 2022].

Natural plant-based fibres, despite their advantages, perform poorly in concrete when in contact with cement hydration if not treated. This is mainly due to their highly hydrophilic nature [Zhang et al., 2013], which negatively impacts fibre-matrix mechanical properties [Gonzalez et al., 2023]. However, surface treatment of natural fibres is widely accepted as an effective method to enhance the performance of natural fibre-reinforced concrete. Javadi et al. [2010] and Fernandes et al. [2013] have reported the positive effects of chemical treatment on natural fibres. Consequently, several studies, including Mansur [1982], Sgriccia et al. [2008], Bera et al. [2010], Ahmad et al. [2022], and Hait et al. [2024], have demonstrated that chemical treatment improves the mechanical properties of natural fibre-reinforced concrete composites.

Over the past three decades, numerous studies have successfully integrated natural fibres into concrete composites. However, there is a notable gap in studies that focus on incorporating natural sponge fibres into concrete composites. This study aims to investigate the effects of both untreated (NonC) and sodium hydroxide (N)-treated NSF on the microstructure, diffusion, and mechanical properties of NSF-reinforced concrete (NSFRC) beams, as well as their environmental benefits.

2. EXPERIMENTAL TEST SETUP

2.1. Materials

The materials used for the concrete mixtures, the mixture ratio, and the mixture proportions, as well as mixing procedures, can be found in Kassum and Acquaye [2024].

2.2. Beam specimens' preparation

The mix proportion, fibre contents, and treatments used for the beam specimens were consistent with those published by Kassum and Acquaye [2024]. A mould-box with dimensions of 100 mm (width), 100 mm (depth), and 500 mm (length) was used for casting the beam specimens. The moulds were cleaned and oiled before use. After verifying workability, the concrete mix was poured into the moulds in two layers. Each layer was compacted for 30 seconds or more using a vibrating table. The filling process involved three increments, with the middle increment being twice the volume of the first and last increments (see Figure 2). The second layer was topped up, levelled with a float, and vibrated for an additional 30 seconds. Each of the two mixed groups, with three fibre contents, along with the mass concrete, was prepared in triplicate. A total of 21 beam specimens were cast, covered for 20 hours, and subsequently prepared for flexural testing. Prisms and core discs were later extracted from these specimens for testing their axial compressive strength and durability, respectively.

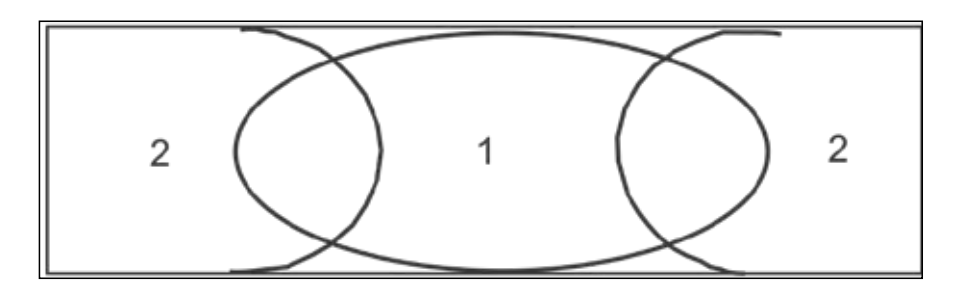


Figure 2. The order of filling the beam mould

Curing of the beam specimens was performed after 20 hours of casting. The beam specimen was demolded and placed in a water-curing tank at 18 °C for 28 days, after which it was tested. Curing was observed in accordance with standards such as BS EN 12390-2 (see Figure 3).

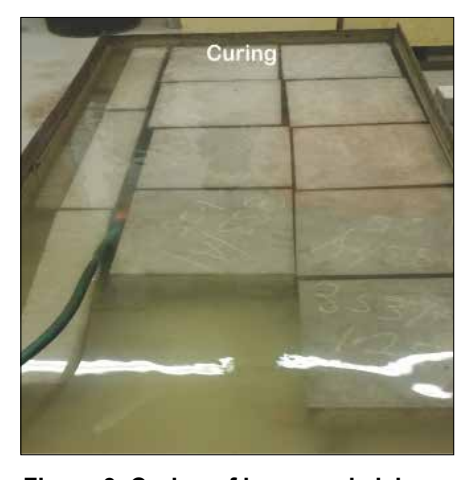


Figure 3. Curing of beam and slab specimens.

2.3. Flexural test procedure

The second phase involved flexural testing of 100 x 100 x 500 mm beam specimens, conducted in compliance with SANS 5864 and BS EN 12390-5:2019 standards under a four-point bending configuration. The tests used an Avery-Dension LS10DE, 7122/3374 testing machine calibrated with notches attached to the plate holding the two upper rollers. The hydraulic Zwick/ Roell Z00 equipment operated with a maximum load capacity of 2000 kN and a loading of 6 kN/min. The beams were positioned on two supporting rollers spaced 100 mm from each end. The two upper rollers were lowered onto the beam specimens at 200 mm from each end.

A controlled force of 6 kN/min was automatically applied until crack initiation, and eventual failure modes were observed in specimens of NSF-reinforced concrete and mass concrete after each trial. The deflections were recorded incrementally via sensors as loading progressed. The maximum load was recorded to calculate the flexural strength using Equation 1. The experimental setup is illustrated in Figure 4.



Figure 4. Test setup for beam of NSFC

$$F_{cf} = \frac{Fl}{b(d^2)}$$
 Equation (1)

where is the flexural strength, in megapascals; is the ultimate load at failure, in Newtons; is the distance between the supporting rollers, in millimetres; *b* is the width of the specimen, in millimetres; *d* is the depth of the specimen, in millimetres.

2.4. Extraction of core disc and prism from the failed concrete

As part of durability and service life assessment, specimens were extracted from the good sections of the failed beams following flexural testing. However, the procedure for extracting the core has been detailed in an earlier publication [Kassum and Acquaye, 2024].

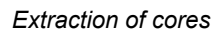
Extraction of prisms. The failed beam specimens were cut to a length of 200 mm using the Geotech GKT/45 machine. The GKT/45 machine operates at a speed range of 500 – 1000 rpm and is equipped with a diamond cutting saw. The ruler on the platform, which holds the specimens, was set to the required length of 200 mm. The specimens were positioned on the platform with a stopper attached to secure them in place. The cutting saw was lowered onto the specimen while in motion to perform the cut. Water was sprayed along the cutting edge to provide cooling during

the process. A total of 21 prisms, each with dimensions of $100 \times 100 \times 200 \text{ mm}$, were prepared for this study (see Figure 5).

2.4.1. CORE DISC EXTRACTION AND PREPARATION.

The processes used to extract the prisms were identical to those used for core discs. Twenty-one (21) cores were extracted from the tested specimens. These thirty (30) cores were cut into discs with a height of 40 mm and a diameter of 100 mm. A total of forty-two (42) core discs were obtained, divided equally into two groups for moisture impact assessment (see Figure 4).







Extracted cores





Cutting of discs and prisms

Extracted prism

Figure 5. Extraction of core disc and prism specimens

2.5. Determination of density

The extracted prism specimens, prepared in triplicate for each fibre-reinforced concrete mix across the two groups, along with the mass concrete, were weighed. A mass-in-air technique was used to determine the density of the specimens. Specimens were weighed using a digital balance, and the average weight of the three triplicates was recorded as the representative density for each mix. Density was calculated according to BS 1881-114 (BSI 1983a), using the formula presented in Equation 2.

$$\rho = \frac{M}{V} \quad \text{Equation (2)}$$

where ρ = density, kg/m³; M = mass, g and V = volume, m³.

2.6. Axial compressive testing procedure

After shaping the fractured faces of the beams to achieve the required dimensions of $100 \times 100 \times 200$ mm, the prism specimens were cured in a water tank for 48 hours following SANS specifications. The bearing surfaces of the specimens were wiped with a damp tissue to ensure proper contact between them. The specimens were then positioned under a compression testing machine with a 5,000 kN load capacity, following SANS 5865 (SABS SM 865) and BS EN 12390-3:2019 standards. A constant loading rate of 0.3 MPa/s was applied during compressive testing of the 21 prisms until failure. The average maximum failure load values were recorded and used to calculate compressive strength using Equations 3. The experimental setup for the compression tests is illustrated in Figure 6.

$$F_c = \frac{P}{A}$$
 Equation (3)

where F_c is prism compressive strength measured to the nearest 0.5 MPa, P is the load at failure, in newtons, and A is the area of the bearing surface of the prism, in square millimetres.



Axial compression testing

Figure 6. Compression setup for prisms.

2.7. Moisture impact and testing

Moisture in fibre-reinforced concrete (FRC) is detrimental to its strength and service life (durability). Diffusion tests were conducted to assess temperature diffusion behaviour in NSFRC, with comparisons made to mass concrete. A total of twenty-one (21) out of the forty-two (42) core discs were used for this test. The core discs were selected without their original orientation (top or bottom). Specimens were ovendried to a uniform average mass (dry weight). Diffusion testing was performed according to ASTM D 570-98 standards. Core discs were fully submerged in distilled water within separate ovens maintained at 23 °C, 60 °C, and 85 °C. At 24-hour intervals, discs were removed, wiped with damp tissue, and weighed (wet weight) before submersion - a process completed within 15 seconds. Water uptake (%) was calculated using Equation 4, with testing continuing until equilibrium mass was achieved for each disc. The diffusion coefficient was then computed using Equation 5 [Espert et al., 2004].

The laboratory setup for diffusion testing is shown in Figure 7.

Water uptake
$$(w_{ph}\%) = \frac{\text{wet sample at time (h)-mass of dry weight}}{\text{mass of dry weight}} \times 100\%$$

Equation (4)

While the diffusion coefficient was computed from

$$D (mm_2/s) = (\frac{l\sqrt{\pi}}{4Me_{\infty}} .slope)^2 Equation (5)$$

where slope is taken from the graph of $\frac{l\sqrt{\pi}}{Me_{\infty}}$. slope) ² Equation (5) where slope is taken from the graph of $\frac{W_{ph}}{Me_{\infty}}$ plotted against h^{1/2} is the specimen

thickness, $W_{_{Dh}}$ is the % of water uptake, $Me_{_{\infty}}$ is the moisture of the equilibrium stage, and D is the moisture molecules diffusion coefficient.

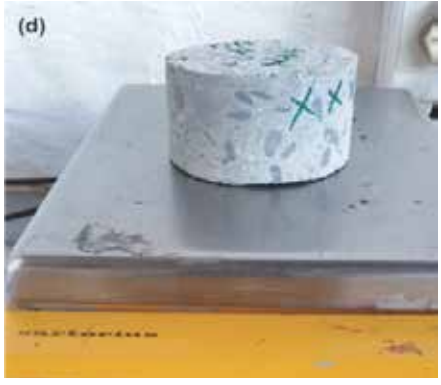




Oven dry of disc

Diffusion set up





Diffusion process, disc in hot water

Weighting of disc



Core discs after diffusion test

Figure 7. Diffusion processes in the laboratory: (a) oven dry, (b) diffusion setup, (c) discs in hot water, (d) weighing of disc, and (e) discs after diffusion

2.8. Microstructure analysis

Fracture surfaces of NSF specimens after immersion temperature test were used to assess their surface quality and dispersion in hardened concrete.

The behaviour of microscopic NSFRC under loading is influenced by the fibres' micromechanics (microstructure) and the surrounding interfacial zone. The fibres' micromechanics or microstructure cannot be understood with the naked eye. Hence, in the decade now, with advancements in microtechnology, an advanced experimental technique like SEM has been invented (see Figure 8). Many have been accepted as an effective technique for determining various microscale material properties [Yan et al., 2015; Vargas et al., 2017]. The SEM took place at the Microscopic and Microanalysis Unit (MMU) on the PMB campus of UKZN. The specimens were examined and analysed using an X-max Zeiss EVOSEM/LS 15/80 mm² SEM device (Germany).

The smallest piece of each specimen was cut and well-shaped, and then mounted on aluminum stubs numbered secured with double-sided electrically conductive adhesive tape. The SEM operated at an acceleration voltage of 5.00 kV with a working distance of approximately 9.0 mm and a vacuum chamber pressure of $3.30 \times 10^{\circ}$ (-3) Pa. The samples were sputter-coated (30 mA) for 30 seconds with a thin layer of gold to make them conductive, and then placed in a vacuum chamber for examination. However, the coating prevents direct contact with the electric charging from reaching the samples. An electronic ray reacts with the samples, generating several types of signals that transform into an image. The SEM images were then moved gradually using a rotating ball to improve their quality. The images were then acquired at magnifications of 48x, 200x, 500x, and 1000x, and subsequently digitized at 2560 x 1920 pixels with resolutions of 10 µm and 20 µm. A Secondary medium was used to copy the images for analysis.



Figure 8. Scanning electronic microscopic set up (Source: PMB, UKZN)

3. RESULTS AND DISCUSSION

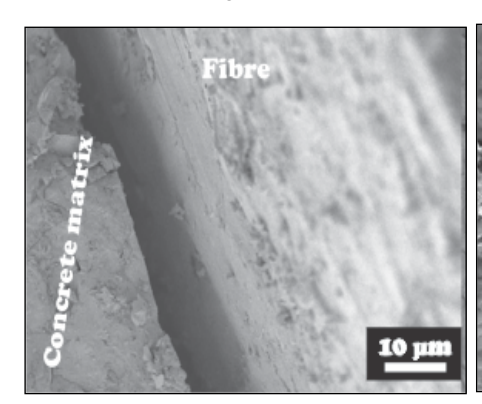
3.1. Material characterisation

The microstructural micrograph of N-treated and NonC-treated fibres, ITZ (Interfacial Transition Zone), and fracture composites surface were discussed in Kassum and Acquaye [2024].

It was concluded that sodium hydroxide treatment effectively removed the hydroxyl substances from the fibre surfaces, thereby enhancing fibre-matrix bonding. This improvement resulted in reduced cracking on the composite surface and a narrower gap in the ITZ.

3.1.1. SEM MICROSTRUCTURAL ANALYSIS OF TREATED NSFRC AFTER TEMPERATURE ENVIRONMENT

Figures 9 (a) and (b) show SEM micrographs of NonC-treated and N-treated NSFRC fracture surfaces after thermal exposure to 85 °C. The SEM micrograph depicts that both NonC-treated NSFRC and N-treated NSFRC (Figure 9) exhibited fibre surface degradation in their microstructures. However, NonC-treated NSFRC showed more severe degradation compared to N-treated NSFRC, as evidenced by irregularities in fibre-matrix bonding and surface erosion.



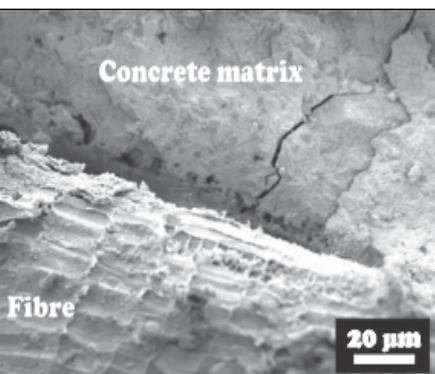


Figure 9. SEM micrograph of (a) NonC-treated and (b) N-treated NSFRC fracture surface after 85 °C

The NonC-treated NSFRC surface exhibited a dizzy appearance and loss of structural integrity (surface texture), indicating poor fibre-matrix interfacial bonding. This observation suggests that the resistance to hot water exposure was compromised, leading to reduced resistance to moisture diffusion. In contrast, N-treated NSFRC demonstrated superficial degradation but outperformed NonC-treated NSFRC due to the enhanced protective properties of the treatment solution. It has been reported that concrete mixtures reinforced with fibres that are scattered significantly reduce the incidence of cracks caused by thermal temperature [Li et al., 2022]. Hence, N-treated NSFRC specimens can be used.

3.2. Concrete properties

3.2.1. PHYSICAL PROPERTIES OF NSFRC

The workability for concrete prepared using 0.00%, 0.75%, and 1.25% of NonC and N-treated NSF is discussed earlier in Kassum and Acquaye [2024]. It was found that the addition of N-treated NSF in the concrete resulted in lower slump values compared to their counterparts. It was concluded that the surface quality could account for the variations in the slump values.

Figure 10 shows the dry density of CTRL concrete, NonC, and N-treated NSFRC prisms. The results indicate that the addition of NSF adversely affected the density of CTRL concrete prisms. Among the NSFRC prisms, N-treated specimens recorded the lowest density values, with approximately 8.47%, 6.29%, and 5.12% reductions relative to the control for fibre contents of 0.75%, 1.00%, and 1.25%, respectively. This trend could be attributed to improved interfacial transition zone properties between N-treated fibres and the cement matrix, which reduces interfacial gaps. Fewer voids likely lowered water absorption, thereby increasing specimen mass. These findings align with Ozerkan et al. [2013], who emphasized that effective

fibre treatment enhances bonding at the fibre-matrix interface.

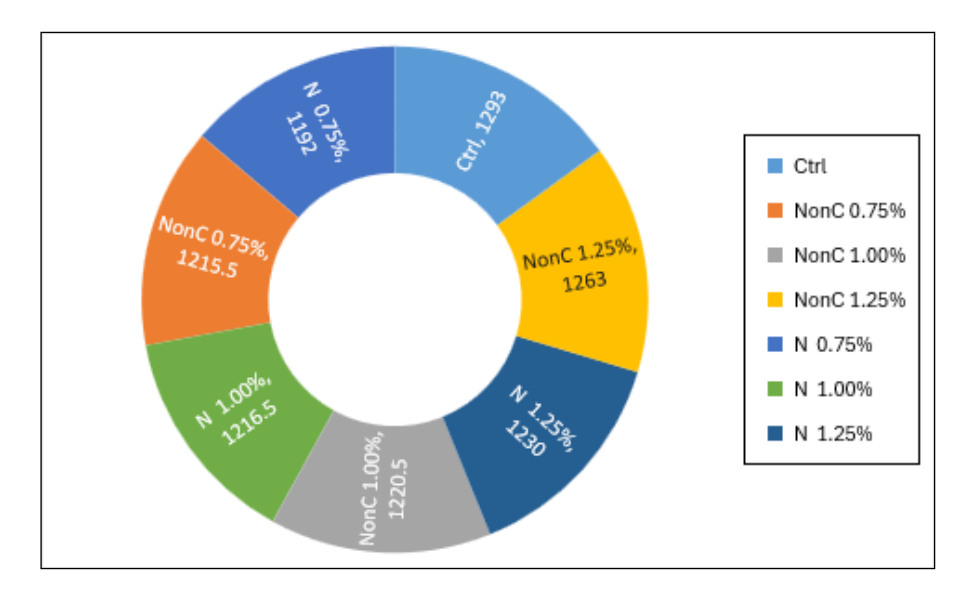


Figure 10. Density of CTRL and NSF hardened concrete prisms

3.3. Hardened properties of NSFRC

3.3.1. INFLUENCE OF TREATMENTS ON FLEXURAL STRENGTH OF NSFRC BEAMS

The average results for CTRL concrete, NonC, and N-treated NSFRC beams tested for flexural behaviour are shown in Figure 11. The figure demonstrates that sodium hydroxide (N) treatment significantly enhanced NSFRC beam performance across all fibre contents, with values consistently surpassing those of the NonC-treated counterpart. The flexural strength improvement correlates directly with effective fibre treatment. The CTRL concrete served as a transitional benchmark, distinguishing between high and low performance in NSFRC beams. Close examination of Figure 10 reveals that NonC-treated NSFRC beams exhibited the lowest flexural strength among all groups, with values of approximately 140% (MPa), 185% (MPa), and 200% (MPa) for fibre contents of 0.75%, 1.00%, and 1.25%, respectively.

In contrast, N-treated NSFRC beams recorded markedly higher flexural strength gains relative to CRTL concrete. Specifically, their values exceeded those of NonC-treated beams by margins of 75%, 45%, and 45% for fibre contents of 0.75%, 1.00%, and 1.25%, respectively.

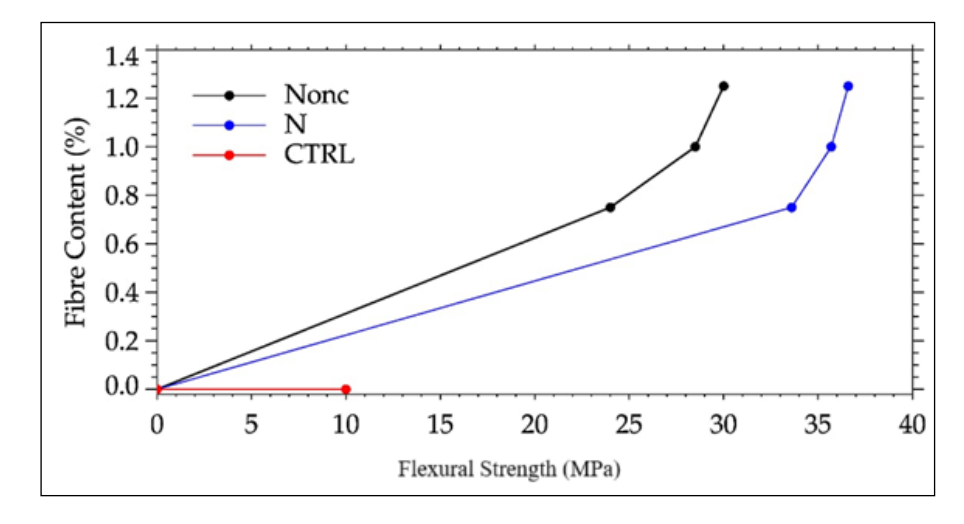


Figure 11. Impact of NSF treatments on flexural strength

The disparity in flexural strength between NonC-treated and N-treated NSFRC beams stems from differences in fibre-matrix adhesion. Non-C-treated NSRFC beams exhibited frail border layers on their fibre surface, which prevented adequate bonding with the cement matrix. Consequently, these composites failed to withstand vertical stress-induced strain, resulting in the lowest flexural strength due to inadequate protection from the concrete.

However, N-treated NSFRC beams benefited from the bleaching action of sodium hydroxide, which reacted with hydrophilic hydroxyl groups on the fibres. This process removed the frail border layers, inducing hydrophobicity and enhancing fibre-matrix interfacial bonding. The improved adhesion enabled superior load transfer, yielding the highest flexural strength in hardened concretes.

3.3.2. LOADING EFFECTS AND DEFLECTION OF NSFRC BEAMS

Figure 13 presents the mean results of the load-deflection curves of the treated NSF from the flexural testing, which shows the varied treatment effect on the beam specimens. Twenty-one concrete beams with fibre contents of 0.00%, 0.75%, 1.00%, and 1.25% were moulded, each containing all the treatments. Figure 13 illustrates that treatments impact the relationship between the load and deflection curves of NSFRC beams. The results showed that, at the beginning of the flexural loading, to about 50%, the beams exhibited linear elastic behaviour on the load-deflection curves. As the flexural loading on the beams increased to about 85%, the natural sponge fibres within the beams, which are located in the tension zone and under the influence of vertical stresses, reached the upper yield point and began to undergo plastic deformation (deflection), leading to the first initial crack. The flexural loading rate of increase slowed down to its maximum stage due to a change in the fibres' curvature, whereas the deformation increased at a faster rate. Due to the

M+N treated

quicker deformation rate at the maximum stage, the natural sponge fibres pulled out, leading to widening cracks in the lower surface of the beams (see Figure 12). Beyond the maximum stage, the beams reached a stress level at failure as the flexural loading began to decline to zero. Based on this explanation, the various concrete beams made are discussed below.



N treated

Figure 12. Deformation of tested NSF reinforced concrete beams

Dw treated

Based on the explanation, the failure posture of CTRL concrete beams was as expected for mass concrete since its maximum load was the least and failed at the first crack.

Within the fibre concrete beams, NonC-treated NSFRC beams failed in shear at their maximum stress, which is almost the same as the CTRL composites. The NonC-treated NSFRC beams failed after the first crack at their maximum stress without additional load, exhibiting a brittle failure mode. The beams resulted in the highest deflection with the most widening cracks, followed by stiffening behaviour in the failure stage. From Figure 13, the NonC-treated NSFRC beams decreased to 43.75%, 42.11%, and 30% of their maximum stress capacity in their fibre contents at 0.75%, 1.00%, and 1.25%, respectively. The reason is that non-chemically treated natural fibres possess many hydroxyl groups, which impede effective fibre interaction with the cement matrix. The hydroxyl groups created non-frictional resistance at the fibre's surface, resulting in significant fibre pull-out, reduced maximum stress capacity, and weak failure. The literature confirms that the behaviour of hydrophilic fibres is poor in flexure unless they are chemically treated [Bessadok et al., 2009].

The treatment of N-composites on NSF positively influenced the load-deflection curves (results) of all the fibre contents compared to NonC-composites. The N-treated NSF in the concrete beams improved their loading carrying capacity. After the first crack, the N-treated NSFRC beams retained their strength as the flexural loading continued. However, at their maximum stress, failure in crushing occurred in the flexural loading region. The N-treated NSFRC beams exhibited lesser deflections with narrow cracks, followed by strain-softening behaviour due to the effectiveness of fibre bridging. The N-treated NSFRC beams exhibited a decreased deflection in all their fibre contents, with 13.91% of their maximum stress capacity at a fibre content of 1.25%. The reason is attributed to removing the hydrophilic contents (hydroxyl groups) from the fibre's surface, as confirmed by sodium hydroxide treatment in Kurpińska et al. [2022]. The fibres exhibit a robust interfacial bonding that enhances the beams' maximum stress capacity and results in gradual and lower deformations within their fibre contents, characterized by an unstiffening strain behaviour during the failure stage, as shown in Figure 13.

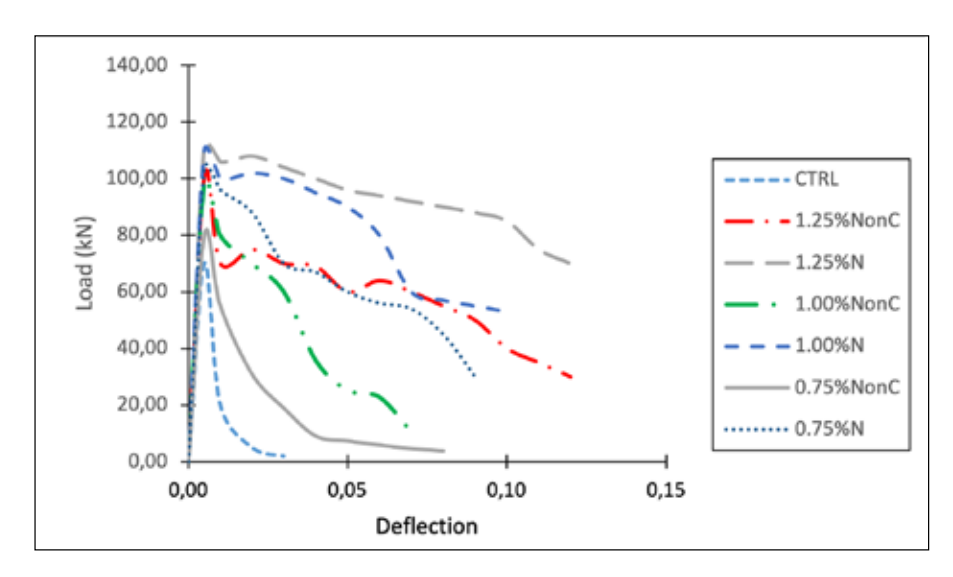


Figure 13. Typical load-deflection behaviour of varied NSF treatments reinforced concrete beams

3.3.3. FLEXURAL STRESS-STRAIN CURVES OF NSFRC BEAMS

Figure 14 shows the stress-strain behaviour of CTRL and NSFRC beams under flexural loading. During flexure, vertical compressive stresses act on the beam's upper surface, while the horizontal tensile stresses develop on the bottom surface. As the upper surface contracts, fibres between the loading rollers transition from a linear alignment to curvature toward the neutral axis. This curvature induces microcracks at the frail fibre-matrix interface due to fibre movement toward the neutral axis. Conversely, the bottom surface expands in length below the neutral axis, causing fibres to curve outward. Continual fibre bending at the point, driven by increasing vertical stresses (flexural loading), caused fibres above the neutral axis to curve outward due to strain transfer from the bending fibres. Simultaneously, the beam's lower surface below the neutral axis experienced severe horizontal tensile stresses due to irregularities at the fibre-matrix border and the matrix inhomogeneity above the neutral axis. This interface conflict between the fibre-matrix led to crack initiation on the lower beam surface. As a result, the fibres transitioned beyond the linear elastic stage into plastic deformation, progressing to a maximum stress and ultimately reaching the failure stress. Figure 14 illustrates this progression, depicting NSFRC beams subjected to identical flexural testing protocols.

Figure 14 shows the typical flexural stress-strain curves derived from the average results of the flexural test. The beam composites' average results were analysed by calculating the area under the stress-strain curve using a spreadsheet. It is observed that all curves showed linear behaviour during the initial elastic stage before transitioning to inelastic deformation. Additionally, the results, as shown in the graph, suggested that chemical treatment had a positive influence on the stress-strain response, thereby enhancing structural performance.

As shown in Figure 14, the CTRL concrete curve exhibited a nosedive immediately after reaching maximum stress, demonstrating no post-peak toughness. For the NonC-treated NSFRC beams, the stress-strain curves showed linear elastic behaviour during the initial flexural loading stage (vertical stress) up to flexural strengths and strain corresponding to approximately 1.0 MPa: 0.0015, 1.3 MPa: 0.0025, and 1.5 MPa: 0.0041 in fibre content at 0.75%, 1.00% and 1.25%, respectively. The curves deviated from linear elastic to inelastic behaviour up to maximum stresses of 24 MPa, 28.5 MPa, and 30 MPa for 0.75%, 1.00% and 1.25%, respectively. With increasing flexural loadings, the curves declined to failure in the post-cracking

zones. Based on the preceding analysis, NonC-treated NSFRC beams under flexural loading demonstrated severe curvature accompanied by vertical crack development at the fibres' weak interface. This behaviour arises from debonding between curved fibres and the cement matrix, driven by poor interfacial adhesion. Deformed fibres induced extra strains on the adjacent fibres' borders above the neutral axis. As vertical cracks propagated, the lower surface of the beams experienced severe horizontal tensile stresses. At this stage, the beams underwent intensified stresses. particularly concentrated at the lower surface. The coupling effects of vertical cracks and severe horizontal tensioning led to wider crack propagation, culminating in tensile fibre failure at the beams' lower surface.

In the post-cracking stage, no residual fibre reinforcement remained to stabilise the failure fracture due to weak fibrematrix bonding at the interface. As a result, the stress rapidly declined uncontrollably from maximum stress to failure stress, reflecting a loss of structural integrity. NonC-treated NSRFC beams exhibited the lowest maximum stress among their counterparts, as evidenced by minimal ductility in the post-cracking zone. The ineffective interface between NonC-treated NSF fibres and the cement matrix stems from frail fibre borders. These fibres retain hydrophilic surface contaminants (e.g., hydroxyl groups) that impede adhesion, resulting in minimal frictional resistance matrix deformation. against weakness reduces the beams' maximum load-bearing capacity and decreases their flexural strength, culminating in brittle failure behaviour characterised by sudden structural collapse. Fidelis et al. [2013] demonstrated that fibre morphology critically influences mechanical performance. Untreated natural fibres exhibited weak interfacial bonding, as observed in brittle failure behaviour, as reported by Lam and Yatim (2015), where structural collapse occurs suddenly without ductility.

However, N-treated NSFRC beams demonstrated superior flexural stressstrain curves compared their exhibited counterparts. The beams higher-yielding sustained curves, proceeded maximum stress, and smoothly into the post-cracking zone. During the initial phase, the stress-strain curves remained linearly elastic up to flexural strengths of approximately 0-1.3 MPa, 0-1.5 MPa, and 0-1.9 MPa for fibre contents of 0.75%, 1.00%, and 1.25%, respectively. At this stage, both beams and fibres exhibited linear behaviour. Under repeated flexural loadings, the stress-strain curves deviated from linear elastic to inelastic behaviour up to maximum stresses of 0 - 3.15 MPa, 0 - 3.3 MPa, and 0 - 3.45 MPa for fibre contents of 0.75%, 1.00% and 1.25%, respectively. Following this peak, the curve exhibited a gradual decline. As evident from these results, NonC-treated NSFRC beams showed an increase in flexural strength. This enhancement was attributed to the removal of hydroxyl groups from the fibre surfaces, which previously acted as impediments. This finding is supported by the literature, as noted by Mahjoub et al. [2014]. As a result, the fibres became cleaner and rougher, enhancing their ability to form stronger interfacial bonds with the cement matrix. This improvement resulted in increased frictional resistance against the matrix, improved sustenance under flexural loading, and enhanced stress transfer capability. Ultimately, the beams showed improved flexural strength and ductility. During flexural loading, the fibres on the upper surface of the beams, above the neutral axis, exhibited minimal deviation from linear elastic to inelastic behaviour, even under increased vertical stress.

On the other hand, the beam's lower surface changes to an inelastic state with reduced curvature. Due to the treatment, irregularities at the fibre-matrix interface above the neutral axis did not induce significant strain on the fibres below the neutral axis, resulting in minor vertical cracking. For this reason, the combination of vertical cracks and resultant horizontal tensile stresses resulted in minimal tensile failure in

both fibres and beams. This outcome occurred as the matrix transitioned from linear elastic to plastic deformation, thereby mitigating severe structural failure. The result was a failure characterised by minimal cracking on the beam's lower surface. It was observed that flexural loading started to decline steadily after reaching maximum capacity, a phenomenon confirmed by Mohsin et al. [2014].

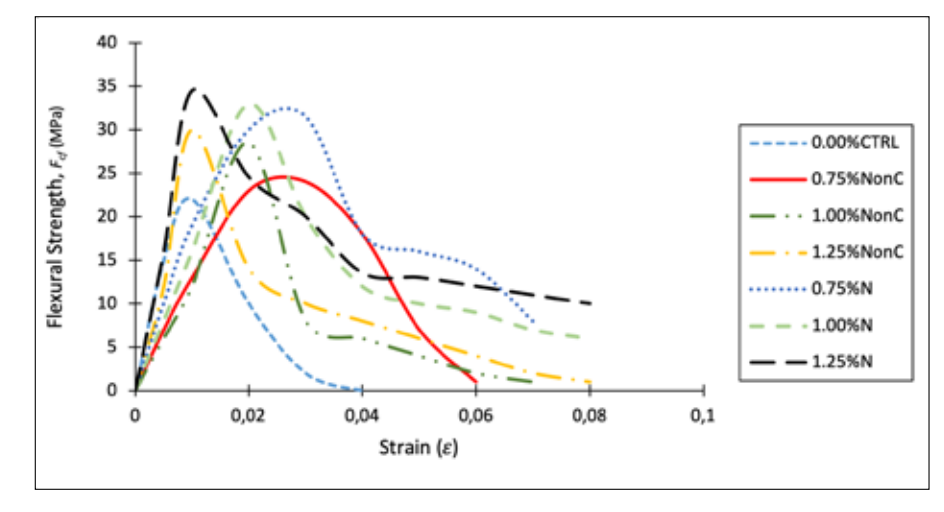


Figure 14. Typical flexural stress-strain relationship of treated NSFRC beams

3.3.4. TENSILE ELONGATION OF BEAM COMPOSITES REINFORCED WITH NSF

Figure 15 illustrates the tensile elongation behaviour of CTRL and treated NSFRC beams under vertical loading. Elongation was determined by measuring the failure length (tension zone) as a percentage of the original length, with mean results plotted in Figure 15. This analysis aimed to assess the influence of treatments on tensile elongation at failure. Within the figure, NonC-treated NSFRC beams exhibited the highest tensile elongation across all fibre contents: 0.05 (5%), 0.044 (4.4%), and 0.032 (3.2%) for 0.75%, 1.00% and 1.25% fibre content, respectively, after the CTRL concretes. The composites exhibited more extended crack widths due to ineffective fibre-matrix bonding, driven by the presence of hydrophilic hydroxyl groups on the fibre surfaces. These impurities acted as impediments, weakening fibre-matrix adhesion. During flexural loading, fibres could not withstand strain, resulting in longer cracks and higher elongation.

Unlike NonC-treated NSRFC beams, N-treated NSRFC beams were better in terms of elongation. N-treated composites exhibited significantly reduced crack widths, approximately 4%, 3.6% and 2% lower than NonC-treated counterparts. This improvement highlights the effectiveness of sodium hydroxide (NaOH) treatment in removing hydroxyl groups, promoting hydrophobicity, and improving fibre dispersion. Enhanced bonding allowed stress transfer to fibres, reducing deformation and crack propagation. The trend line confirmed the impact of treatment on tensile elongation. The R2 value indicates that approximately 67% of the change in tensile elongation can be attributed to the treatment.

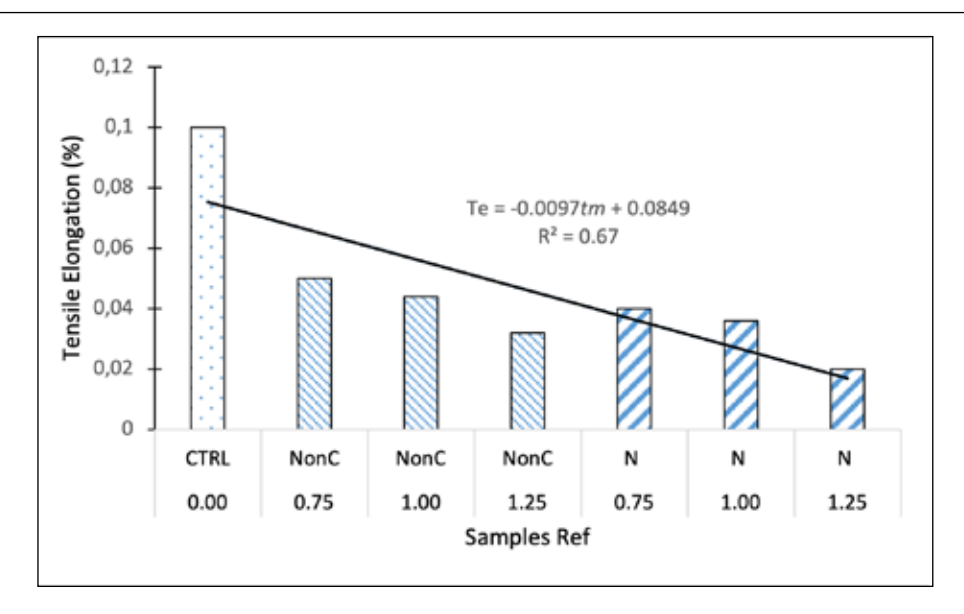


Figure 15. Relationship between treated NSF and tensile elongation at break

3.3.5. FLEXURAL MODE AND PATTERN OF FAILURE OF NSFRC BEAMS

Figure 16 illustrates the failure modes of beam specimens under flexural testing, highlighting the impact of treatment on fibre performance. NonC-treated NSFRC beams exhibited failure progression from crushing to shear, with cracks widening significantly at mid-span. Within the composite, shear failure dominated, with widened cracks and fibre pull-out. Hairline cracks and debonding preceded crushing as a failure pattern. Unlike N-treated beams, the two halves of the beam could not remain bridged post-failure due to insufficient fibre bridging, resembling the behaviour of CTRL composite specimens. The inability to retain structural integrity stemmed from a poor quantity of fibre surface, which hindered adequate fibre-matrix adhesion. N-treated NSFRC exhibited crushing with reduced crack widening, attributed to enhanced fibre-matrix bonding.

Concrete subjected to vertical stresses (flexural loading) is considered a failure when the load declines to 80 – 85% of its maximum stress capacity, as reported by Gao et al. [2020]. This failure mode is characterised by fibre debonding, driven by the propagation of horizontal cracks initiated at the loading region. The orientation of the cracks depends on the fibre-matrix interface and the induced stress distribution. It is observed that N-treated NSFRC beams failed at their mid-span, with cracks developing in the flexural loading region of the beam surface. The failure progressed to crushing, accompanied by hairline cracks at mid-span that remained partially bridged at maximum load due to fibre bridging effects. N-treated beams exhibited superior crack widening resistance compared to untreated counterparts, attributed to reduced fibre pull-out and enhanced control of crack propagation. Ramli et al. [2013] corroborate that chemically treated natural fibres mitigate crack propagation through improved interfacial bonding. The least vertical cracks or crack width may be attributed to the fact that the fibres are effectively aligned in a longitudinal direction, where the applied loading also acts perpendicular to the direction of fibre reinforcement [Yan and Chouw, 2015].





Figure 16. Flexural mode and pattern of failure for (a) CTRL, (b) NonC, (c) N-treated NSRFC beams

3.3.6. AXIAL COMPRESSION STRESS-STRAIN CURVE ANALYSIS

Fibres subjected to repeated axial compression undergo three distinct behavioural stages: linearly elastic, inelastic/plastic deformation, and failure. Ranganathan et al. [2019] explained that reinforcements within concrete prisms transition to lateral inelasticity under instantaneous axial compression, where cracks develop at the reinforcement's vulnerable interface. Fleck et al. [1995] further explained that curvature-induced strain in reinforcements destabilises adjacent regions, causing the concrete reinforcement interface to deviate from linear elasticity to inelasticity. Prolonged strain progression leads to post-inelastic behaviour, exceeding maximum stress before eventual failure.

Therefore, the study discusses average test results from prisms extracted from deformed beams. The compressive stress-strain curves are illustrated in Figure 17, highlighting the behavioural patterns of reinforced and unreinforced specimens in the three stages.

A total of 21 FRC prisms (dimensions: 200 mm in length, 100 mm in breadth, and 100 mm in height) were tested and evaluated for their compressive stress-strain behaviour, compared to the CTRL concrete prisms. Figure 17 shows the average compressive stress-strain curves for CTRL, NonC-treated, and N-treated NSFRC prisms.

The curves exhibited distinct profiles, though all demonstrated linearly elastic behaviour during the initial axial compression stage. The CTRL concrete prism curve failed suddenly, resembling conventional concrete's brittle stress-strain response. For NonC-treated NSFRC prisms, the linearly elastic phase recorded stress ranges of 0 – 7 MPa, 0 – 5 MPa, and 0 – 8 MPa, corresponding to strain of 0.008, 0.007, and 0.004 at fibre enhancement of 0.75%, 1.00% and 1.25%, respectively.

As axial compression increased, composite fibres buckled and matrix cracks initiated due to insufficient stress-strain dominance, resulting in premature failure at a reduced load-carrying capacity. This resulted in truncated stress-strain curves at peak stress.

In contrast, the compressive stress-strain curves exhibited the highest stress with a softening behaviour. The results indicate that N-treated NSRFC prisms achieved ultimate stress of 33.43 MPa, 31.91 MPa, and 26.45 MPa, corresponding to strains of 0.09, 0.08, and 0.06 for fibre contents of 0.75%, 1.00% and 1.25%, respectively (see Figure 17).

As loading progressed, the N-treated NSF specimens demonstrated a controlled decline in stress after reaching maximum stress, ultimately failing with minimal abruptness. Among all tested groups, N-treated NSFRC prisms recorded the highest maximum stress at equivalent fibre contents. This higher performance is attributed to prolonged axial compressive stress-strain curves at peak load and enhanced softening behaviour, reflecting greater dominance in stress-strain response compared to other prisms.

The variations in maximum stress and curves occur during axial compression. The loadings on the N-treated NSFRC prisms sustained the highest stress at the linear elastic limit without buckling due to their stronger border. With the constant increase in the axial compression loadings, the stronger border zone of the fibres in N-treated NSFRC prisms entered the inelastic stage with minor inelastic buckling. The inelastic buckling was so narrow that minute matrix cracks were initiated in the specimens. At the prism edges, N-treated NSF experienced strains arising from the combined effects of inelastic buckling and matrix cracking. These fibres developed resistance to excessive strain, mitigating severe inelastic buckling and surface crack propagation. Consequently, fewer visible cracks formed and propagated laterally toward the concrete's reinforced border zone. Due to the significant improvement in the fibrereinforced concrete's border zone, cracks progressed beyond the prism's maximum stress threshold into post-inelastic buckling, followed by a controlled decline in loadbearing capacity. At failure, the load-displacement curves demonstrated that cracks were restrained by the N-treated NSFs, resulting in a higher peak compressive stress value and improved ductility.

Studies have reported that fibre-reinforced concrete typically buckles under axial compression, with the severity of the buckling dependent on the properties of the fibre reinforcement. Chemical modification of fibre surfaces enhances bonding with the cement matrix [Mahjoub et al., 2014; Yan et al., 2016].

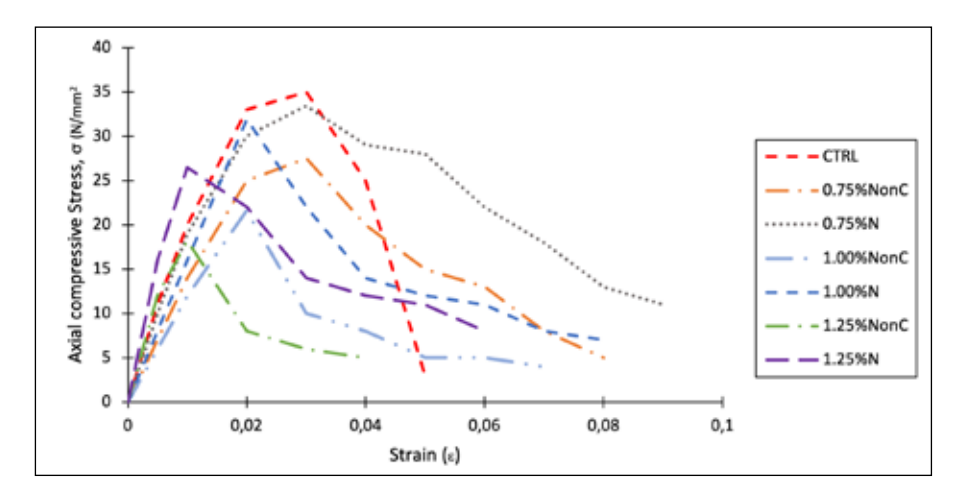


Figure 17. Axial compression stress-strain curve of concrete with NSF, in different treatments

3.3.7. AXIAL COMPRESSION TOUGHNESS RELATIONSHIP

Toughness was calculated using experimental data within the stress-strain area (strain range: 0.00 - 1.2), defined as the energy absorption capacity. The energy absorption capacity of the CTRL, NonC-treated, and N-treated NSFRC prisms is illustrated in Figure 18.

The study revealed the trend in toughness, as measured by compressive energy absorption capacity, as shown in Figure 18. The mass concrete prisms exhibited the highest absorption values, followed by N-treated and then NonC-treated NSFRC prisms. Non-C-treated NSFRC prisms recorded average energy absorption capacity values of 43.5% (J), 48.53% (J), and 50.27% (J), which are lower than those of their N-treated counterparts at fibre contents of 0.75%, 1.00%, and 1.25%, respectively. The variation in absorption capacity is attributed to differences in fibre surface characteristics. The CTRL concrete prisms exhibited higher compressive strength due to the presence of fewer voids in the composite. Non-C-treated NSFRC prism contained higher cellulose content, which acted as an impediment to fibre-matrix adhesion, increasing void formation. As reported by More and Subramanian [2022], poor fibre-matrix bonding, often caused by surface impurities, weakens compressive performance. Conversely, N-treated NSF fibres demonstrated improved adhesion, reducing voids and enhancing energy absorption. Hence, it exhibited the largest toughness surface.

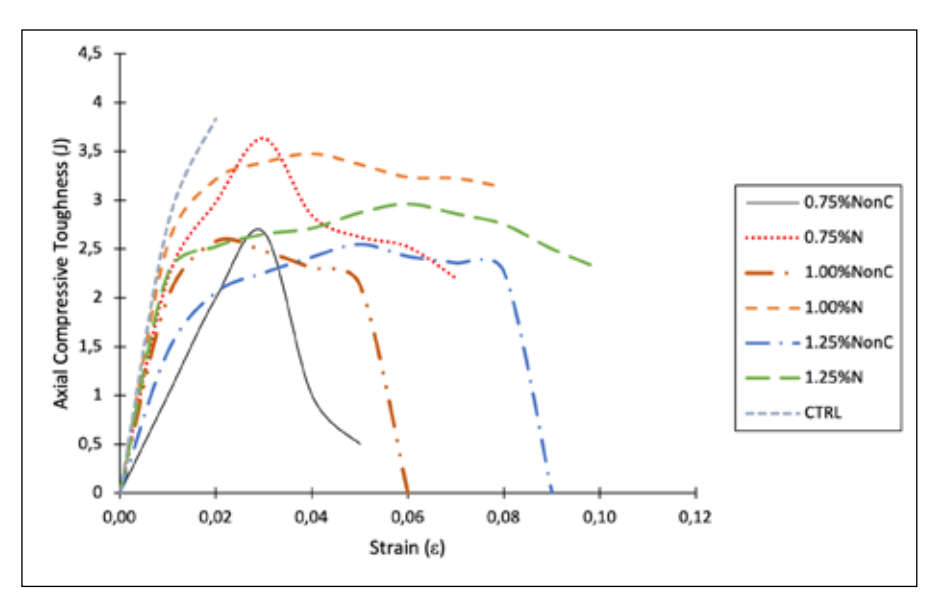


Figure 18. Toughness-strain curve of concrete with NSF, in different treatments

3.3.8. THE MODE OF FAILURE OF THE NSFRC PRISM UNDER AXIAL COMPRESSION

Figure 19. shows the failure modes of the CTRL concrete prism and NSFRC prisms with varying treatments under axial compression. Figure 19 (a), (b), and (c) show the CTRL, NonC-treated, and N-treated NSFRC prism, respectively. The CTRL prism exhibited splitting failure due to a lack of bonding among its composite constituents. In contrast, NonC-treated NSRFC prism failed via axial untying cracks – a unique mode distinct from N-treated prisms (see Figure 19 (b)). This failure was linked to the hydroxyl groups in untreated fibres, which compromised fibre-matrix adhesion. During testing, NonC-treated prisms "exploded" at peak stress, recording average failure loads of 27.53 kN, 21.6 kN, and 18.2 kN (ascending order of fibre content: 0.75%, 1.00%, 1.25%).

N-treated NSFRC prisms failed by 'crushing', with cracks initiating at the base and propagating upward along the axial compression axis (see Figure 19 (c)). A severe crushing occurred approximately one-third of the way from the prism base. N-treated NSF fibres restricted crack propagation by stabilising micro-cracks at the edges, delaying splitting. Audible cracking during testing confirmed this gradual failure mode. The superior performance of N-treated prisms is attributed to the removal of hydrophilic impurities, enhancing fibre-matrix bonding. Effective fibre reinforcement reduces the propagation of axial strain beyond the peak stress, thereby improving fracture energy absorption and failure resistance.







Figure 19. Failure mode and pattern of axial compression of (a) CTR, concrete, (b) NonC, and (c) N treated NSFRC prisms

3.3.9. MECHANISM OF FIBRE-MATRIX INTERACTION

The variation in performance between NonC-treated and N-treated NSFRC prisms stems from the chemical action of sodium hydroxide (N). The alkaline solution reacts with hydrophilic hydroxyl groups on fibre surfaces, dissolving H+ and OH- into water molecules and removing them. Residual sodium hydroxide further reacts with the fibre cell wall, forming an amorphous region (a rougher surface morphology) – a process absent in NonC-treated fibres.

This rougher surface enhances fibre dispersion and strengthens fibre-matrix interfacial interlocking, as confirmed by prior studies [Mohanty et al., 2001; Elsaid et al., 2011; Yan et al., 2016; More and Subramanian, 2022]. Improved interlocking enhances the composite's load-bearing capacity, enabling resistance to severe inelastic buckling and aligning with the performance trends observed in earlier figures.

3.4. The water absorption mechanism of NSF-reinforced concrete in varied conditions

The absorption of water directly affects the durability of fibre-reinforced concrete composites; it is one of the conditions responsible for the deterioration of the reinforcement within the concrete the surrounding specimens in environment. Therefore, the average experimental results of CTRL concrete, NonC. and N-treated NSF reinforced concrete core discs at 23°C, 60°C, and 85°C were used to assess the water absorption behaviour and diffusion case, as well as their coefficients.

3.4.1. WATER ABSORPTION CURVE FOR NSF REINFORCED CONCRETE CORE DISCS

Figure 20 shows a graphical representation of the average results of water absorption for CTRL concrete, NonC, and N-treated NSFRC core discs at 60°C. Figure 20 also indicates fibre content of 0.00%, 0.75%, 1.00% and 1.25%. The graph shows the various treatments of fibre concretes subjected to a temperature of 60 °C, compared

to the CTRL concrete. As shown in the graph (Figure 20), a strong positive association exists between treatments and water absorption. The NonCtreated NSFRC specimens recorded the shortest equilibrium time among all the fibre contents when compared to the CTRL specimen.

Regarding water absorption, at the duplicate fibre content with different treatments, the NonC-treated NSFRC with a fibre content of 1.25% recorded a higher water absorption of 13.88% compared to 12.72% for the N-treated NSFRC specimens. It took 12 hours for the fibre content of 1.25% N to absorb 12.7% water content from the fibre content of 1.25% NonC. The results were due to the fibres swelling in the concrete specimens as they absorbed a significant amount of water, attributed to their hydrophilic quality (hydroxyl groups) [Fernandes et al., 2013].

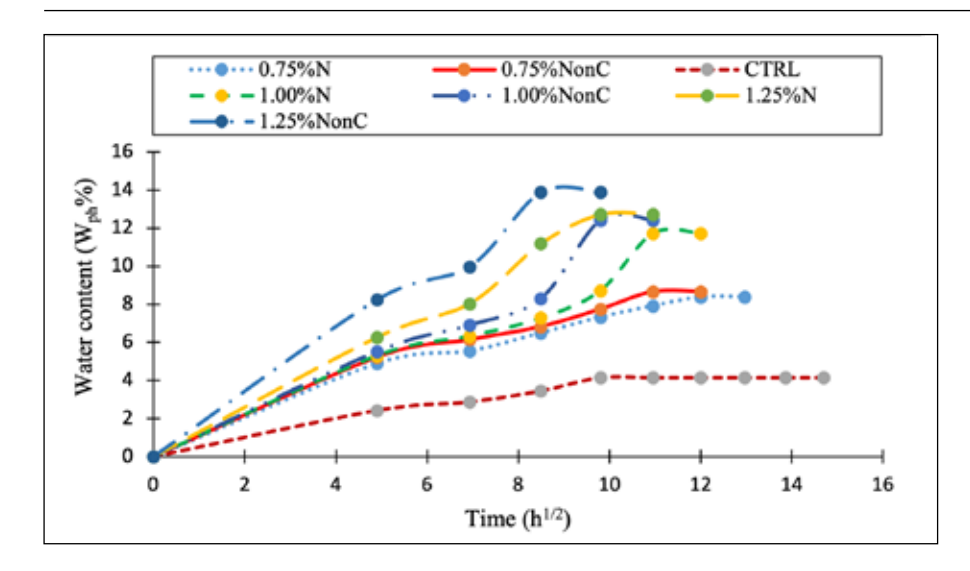


Figure 20. Water absorption curves () for CTRL, NonC, and N-treated NSFRC core discs in water at 60 $^{\circ}\text{C}$

3.4.2. DIFFUSION BEHAVIOUR AND DIFFUSION COEFFICIENTS OF NSFRC CORE DISCS

The diffusion coefficient is the ability of water molecules to move within specimens through the composite's structure. The NSFRC core disc results are shown in typical curves for the diffusion case, after running the results through linear log regression, where the diffusion coefficient is calculated.

Table 1: Mode of Diffusion case and coefficient

Specimens	Diffusion case	Diffusion coefficient
	N	D (mm2/s) x 105
CTRL	0.344	1.14
0.75%N	0.3013	1.70
0.75%NonC	0.3005	1.71
1.00%N	0.4646	1.75
1.00%NonC	0.5366	2.18
1.25%N	0.4882	1.89
1.25%NonC	0.4383	2.25

Equation 6 is Fick's theory that determines which diffusion case the water absorption behaviour that belongs to

$$\frac{W_{ph}}{Me_{..}} = Kt^n \text{ Equation (6) [Espert et al., 2004]}$$

where is the weight of water absorbed at a time; h is the equilibrium water content at saturation. K and n are the model parameters, with K representing the fibre-water interface relationship. Whereas n also demonstrates whether the water absorption behaviour falls under case I, II, or anomalous, with $n = \frac{1}{2}$ for case I. In examining the water absorption, and the diffusion behaviour, by considering logarithmic laws, equation 6 can be transformed into equation 7 by adjusting the laboratory values, allowing n to be calculated.

$$\log \frac{W_{ph}}{Me_{\infty}} = \log^k + n \log^h \quad \text{Equation (7)}$$

Figure 21 presents the average experimental values calculated using equation 5. The values were run in a linear log regression (best-of-fit) in the form, ($\frac{W_{ph}}{Me_{\infty}}$) log h.

The gradient (n) in Table 1, derived from Equation 7, characterises the diffusion behaviour. Results indicate that 1.00% N-treated NSF aligned closely with n= 0.5, consistent with Fickian diffusion (case I). 1.25% N-treated and 1.25% NonC-treated NSFRC specimens also exhibited n = 0.5. However, CTRL, 0.75% NonC, and 0.75% N-treated specimens deviated significantly from n = 0.5. Water absorption data for treated NSFRC core discs with n 0.5 confirm Fickian diffusion behaviour, where moisture ingress follows a one-dimensional, timedependent process governed by Fick's laws [Smith et al,1997; Wikipedia.org; Gibhardt et al., 2023]. This aligns with ISO 62:2008 standards for materials exhibiting Fickian moisture diffusion [BS EN ISO 62:2008; bbsq.bs].

The water diffusion coefficient values were plotted against h1/2. Table 1 shows the water diffusion coefficient of all the specimens from the best-offit part of equation 5. This is the most crucial determinant of Fick's function. Table 1 shows that the percentage of fibre content is directly proportional to the water diffusion coefficient for all fibre specimens, as interfacial voids may have been created, as confirmed by Kufel and Kuciel [2020]. Thus, void engineered the movement of the diffusion agent. Again, treatment is negatively correlated with water diffusion coefficients for the NSFRC specimens, using the CTRL concrete specimens as a reference. Water diffusion coefficients decreased with the inclusion of N-treated NSF. The study has indicated that the N-treated NSFRC specimens recorded the least water diffusion coefficients among all the fibre contents compared to the other counterparts. This difference can be attributed to the better bonding between the treated NSF and the cement matrix. Thereby limiting the transmission of water molecules inside the concrete composite materials due to the elimination of hydroxyl groups. Moshin et al. [2018] have confirmed the positive effects of the treatment.

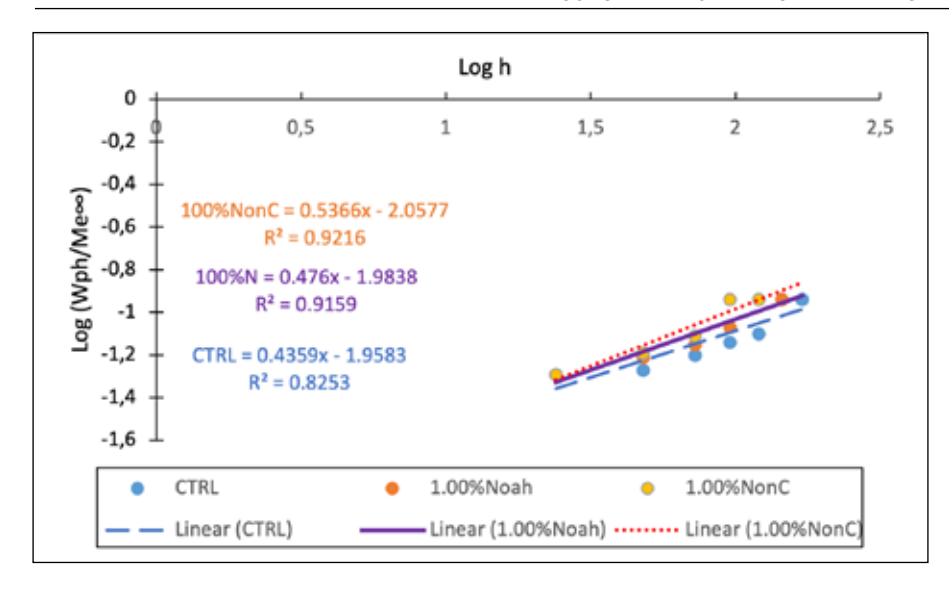


Figure 21. Diffusion case of best-of-fit (slope) for CTRL concrete, NonC, and N-treated NSFRC core discs at 85 $^{\circ}\text{C}$

3.5. The N-treated concrete core discs in varied temperatures

N-treated NSRFC core disc was discussed since in the earlier discussions, it's proven to be better than its counterpart. According to the literature [Ghasemzadeh-Barvarz et al., 2015], the diffusion of water molecules has been identified as one of the primary mechanisms of water penetration into natural fibre-reinforced composites. Additionally, the absorption of moisture into specimens is characterised by the fibre-frail border bonding with the cement matrix. Hence, the water absorption ability at different temperatures for the N-treated fibre content of 1.25% at three varied temperatures (23 °C, 60 °C, and 85 °C) has been graphically plotted in Figure 22.

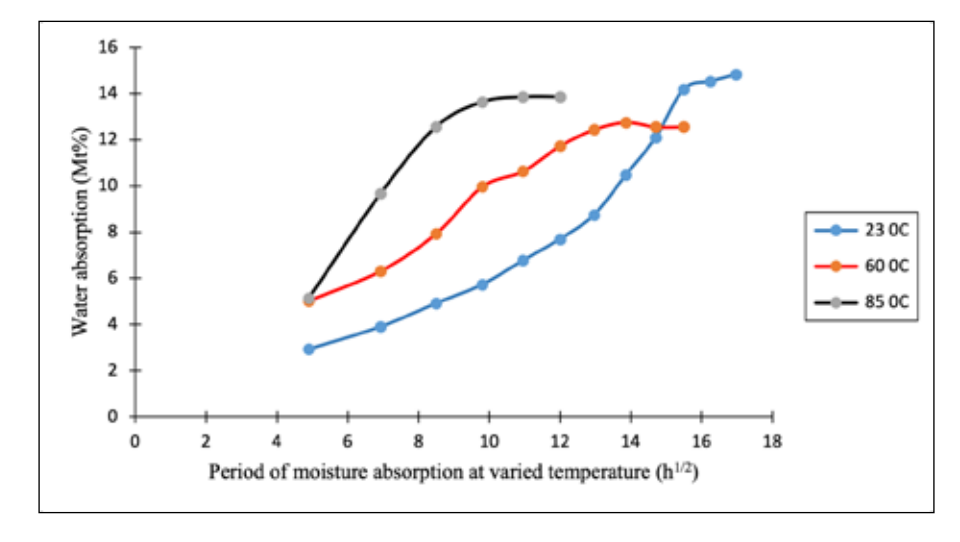


Figure 22. Water absorption curves for 1.25% N-treated NSFRC core discs at varied temperature

From equation 4, the water content difference in dry and wet specimens of the composites is expressed as a percentage of water absorption. The absorbed average water content (%) of the specimens is plotted against the square root of the water absorption time (h1/2) on the graph's axis. Figure 22 shows that the water absorption rate of NSFRC core discs depends on temperature and fibre content. Water absorption (saturation period) is directly proportional to an increase in immersion temperature and fibre content [Wang et al., 2020]. Hence, the elapsed time is shortened. The temperature of 23 °C shows the longest elapsed time, while the temperature of 85 °C shows the shortest elapsed time. The water absorption time is reduced to 144 hours (6 days) after the temperature is shifted to 85 °C from 23 °C. The difference may be attributed to the lighter-weight molecules of the water housing the specimens during heating. which flow freely and more quickly in solids, aligning with Grams and Adolf Fick's laws. The pores in the NSFRC core discs may also have widened in contact with the hot water.

4. CONCLUSIONS

Based on the composites of NSFRC, the following major conclusions can be drawn from this study.

- The addition of NSF decreased the density of NSFRC. Notably, higher-quality N-treated NSF further reduced the density of hardened concrete.
- Temperature variation during hot water curing affects the surface texture of natural fibres in NSFRC. SEM micrographs confirmed variation in treatment efficacy, which directly influenced NSF surface quality.
- Axial compressive-related strength decreased with the increasing NSF content. However, composites reinforced with N-treated NSF showed enhanced load-bearing capacity (stress-strain curves) and their

associated toughness compared to NonC-treated fibres.

- In terms of strength performance, N-treated **NSFRC** beams exhibited highest loadthe carrying capacity and postcracking softening behaviour, consistent with typical fibrereinforced concrete (FRC) mechanics.
- The treatment behaviour and interfacial bonding quality of N-treated NSFRC directly influence its water absorption behaviour, diffusion case, and diffusion coefficient. Elevated temperatures accelerated moisture absorption by reducing the time required for capillary action to occur.
- Based on these findings, sodium (N)-treated NSF hydroxide composites show promise for low-cost housing applications, offering a sustainable solution mitigate climate-related to construction challenges. Future research should investigate alternative chemical treatments to optimize NSF performance further.

5. APPLICATION OF NSFRC

The observed results of the NSFRC treated with sodium hydroxide show its potential as a promising construction material that could serve as an alternative to conventional fibre-reinforced concrete low-cost housing applications. This substitution could reduce the environmental impact associated with conventional fibre production and use in concrete. Based on the findings, however, it is recommended that the hydroxide-treated **NSFRC** sodium should not be used alone for casting the suspended slab and other related structures.

6. ACKNOWLEDGEMENTS

First, the authors would like to express their gratitude to Almighty Allah for the knowledge and their lives, and to Dr. Moses Wopicho Kiliswa and Dr. Oladimeji Benedict Olalusi (Supervisors) for their support and valuable insights. Secondly, the authors would like to express their gratitude to UKZN management, especially Prof. Mustapher (Academic Leader, CAES - Civil), Ishaan Ramlakhan (Chief Technician), Boysie Dumisa (Technician), Logan Govender, Fatima Ali, and Linda (all at UKZN, Howard -SA). Also, the authors would like to thank the following individuals: Dr Dennis Boamah-Boateng and Dr Solomon Otoo Lomotey (UESD) for their editing, Nana Boakye Yam Ababio (Nkwantakese Hene), Nana Otimpie-Aben II (Otumfour Sasaamo panin Hene), Dr Paul Kofi Fynn (Chancellor, Wisconsin International University College, Gh), and Moulana Abdullah Khan (Administrator, Jamiatul Ulama KZN - SA) for their support.

7. FUNDING

No individual or organisation funded this study. However, the University of KwaZulu-Natal (UKZN) provided the authors with access to its facilities.

8. DECLARATION OF INTEREST STATEMENT

The authors declare that there are no conflicts of interest or personal relationships that may have influenced this study.

9. REFERENCES

Abdalla, J. A., Hawileh, R. A., Bahurudeen, A., Jyothsna, G., Sofi, A., Shanmugam, V., & Thomas, B. S. (2023). A comprehensive review on the use of natural fibers in cement/ geopolymer concrete: A step towards sustainability. *Case Studies in Construction Materials*, 19, e02244.

Ahmad, H., Chhipi-Shrestha, G., Hewage, K., & Sadiq, R. (2022). A comprehensive review on construction applications and life cycle sustainability of natural fibre biocomposites. *Sustainability*, *14*(23), 15905.

Ahmad, J., Arbili, M. M., Majdi, A., Althoey, F., Farouk Deifalla, A., & Rahmawati, C. (2022). Performance of concrete reinforced with jute fibres (natural fibres): A review. Journal of Engineered Fibers and Fabrics, 17, 15589250221121871.

American Concrete Institute (2020) RESULTS FOR MASS CONCRETE. Available at: https://www.concrete. org/topicsinconcrete/topicdetail. aspx?search=mass concrete.

Bera, M., Alagirusamy, R. and Das, A. (2010). A study on interfacial properties of jute-PP composites. Journal of Reinforced Plastics and Composites, 29(20), 3155-3161.

Bessadok, A., Roudesli, S., Marais, S., Follain, N., & Lebrun, L. (2009). Alfa fibres for unsaturated polyester composites reinforcement: Effects of chemical treatments on mechanical and permeation properties. Composites Part A: Applied Science and Manufacturing, 40(2), 184-195.

BSI (1983a) BS 1881-114: Methods for determination of density of hardened concrete. BSI, London, UK.

BSI (2009a) BS EN 12390-2: Testing hardened concrete. Making and curing specimens for strength tests. BSI, London, UK, pp. 1–12.

BSI (2019) BS EN 12390-4: Concrete-Tests of hardened concrete-Part 4: Compressive strength-Specification of test machines. Turkish Standards Institute.

BSI (2019) BS EN 12390-4: Concrete-Tests of hardened concrete-Part 4: Compressive strength-Specification of test machines. Turkish Standards Institute.

Elsaid, A., Dawood, M., Seracino, R., & Bobko, C. (2011). Mechanical properties of kenaf fiber reinforced concrete. Construction and Building Materials, 25(4), 1991-2001.

Espert, A., Vilaplana, F., & Karlsson, S. (2004). Comparison of water absorption in natural cellulosic fibres from wood and one-year crops in polypropylene composites and its influence on their mechanical properties. Composites Part A: Applied science and manufacturing, 35(11), 1267-1276.

Fahim, I. S., Elhaggar, S. M., & Elayat, H. (2012). Experimental investigation of natural fibre reinforced polymers. Materials Sciences and Applications, 3(2), 59-66. http://dx.doi.org/10.4236/msa.2012.32009.

Fernandes, E. M., Mano, J. F., & Reis, R. L. (2013). Hybrid cork–polymer composites containing sisal fibre: Morphology, effect of the fibre treatment on the mechanical properties and tensile failure prediction. Composite Structures, 105, 153-162.

Fidelis, M. E. A., Pereira, T. V. C., Gomes, O. D. F. M., de Andrade Silva, F., & Toledo Filho, R. D. (2013). The effect of fibre morphology on the tensile strength of natural fibres. Journal of Materials Research and Technology, 2(2), 149-157.

Fleck, N. A., Jelf, P. M., & Curtis, P. T. (1995). Compressive failure of laminated and woven composites. Composites Technology and Research, 17(3), 212-220.

Gao, D.Y., Gu, Z.Q. & Wu, C. (2020). Bending behaviour and deflection prediction of high-strength SFRC beams under fatigue loading. Journal of Materials Research and Technology, 9(3), 6143-6159.

Ghasemzadeh-Barvarz, M., Duchesne, C., & Rodrigue, D. (2015). Mechanical, water absorption, and aging properties of polypropylene/flax/glass fiber hybrid composites. Journal of Composite Materials, 49(30), 3781-3798.

Gibhardt, D., Buggisch, C., Ahrens, M., & Fiedler, B. (2023). Monitoring of water absorption and its effects on mechanical performance of thick GFRP structures by integrated smart sensors.

Gonzalez, J., Castaño, J. and Puech, F. (2023) 'Tensile strength and drop-weight impact response of polypropylene reinforced with flax and pinewood short fibres', PMC, 13(1), pp. 1-12. Available at: https://pmc.ncbi.nlm.nih.gov/articles/PMC10468331/ (Accessed: 29 October 2024).

Hait, P.R.I.T.A.M., Karthik, R., Mitra, R. and Haldar, R. (2024). Natural and Artificial Fibre Reinforced Concrete: A State-of-art Review. International Journal of Engineering, 37(3), 503-510.

Hasan, K. F., Horváth, P. G., & Alpár, T. (2021). Development of lignocellulosic fiber reinforced cement composite panels using semi-dry technology. Cellulose, 28, 3631-3645.

https://bbsq.bs/product/plasti...

https://www.en.wikipedia.org/wiki/Fick's la...

Ige, O., Barnett, S. J., Nassif, A., & Williams, J. B. (2016, August). Distribution and orientation of steel fibres in steel fibre reinforced concrete. In 4th International Conference on Advances in Civil, Structural and Construction Engineering (pp. 43-47). IRED.

Iso, B. S. E. N. (2008). Plastics— Determination of Water Absorption. Management, 3. https:// www.en-standard.eu Javadi, A., Srithep, Y., Pilla, S., Lee, J., Gong, S., & Turng, L. S. (2010). Processing and characterization of solid and microcellular PHBV/coir fibre composites. Materials Science and Engineering: C, 30(5), 749-757.

Kabir, M.M., Wang, H., Lau, K.T. & Cardona, F. (2012). Chemical treatments on plant-based natural fibre reinforced polymer composites: An overview. Composites Part B: Engineering, 43(7), pp.2883-2892.

Kassum, B., & Acquaye, C. N. A. (2024). Characteristics of natural sponge fibres and their effects on the properties of cement-based materials. Proceedings of the Institution of Civil Engineers-Construction Materials, 1-56.

Kurpińska, M., Pawelska-Mazur, M., Gu, Y., & Kurpiński, F. (2022). The impact of natural fibers' characteristics on mechanical properties of the cement composites. Scientific Reports, 12(1), 20565.

Lam, T. F., & bin Mohamad Yatim, J. (2015). Mechanical properties of kenaf fibre reinforced concrete with different fibre content and fibre length. Journal of Asian Concrete Federation, 1(1), 11-21.

Li, L., Zhang, Y., Shi, Y., Xue, Z., & Cao, M. (2022). Surface cracking and fractal characteristics of cement paste after exposure to high temperatures. Fractal and Fractional, 6(9), 465.

Li, S., Bashline, L., Lei, L., & Gu, Y. (2014). Cellulose synthesis and its regulation. The Arabidopsis Book/American Society of Plant Biologists, 12, e0169. (Accessed: 29 October 2024).

Mahjoub, R., Yatim, J. M., Sam, A. R. M., & Hashemi, S. H. (2014). Tensile properties of kenaf fibre due to various conditions of chemical fibre surface modifications. Construction and Building materials, 55, 103-113.

Mansur, M. A. and Aziz, M. A. (1982). A study of jute fibre reinforced cement composites. International Journal of Cement Composites and Lightweight Concrete, 4(2), 75-82.

Maturix (2023) What is mass concreting? Available at: https://maturix.com/knowledge-center/what-is-mass-concreting/#:~:text=Mass concreting involves using large, to traditional concrete construction methods.

Mohanty, A. K., Misra, M., & Drzal, L. T. (2001). Surface modifications of natural fibres and performance of the resulting biocomposites: An overview. Composite interfaces, 8(5), 313-343.

Mohsin, S. M. S., Azimi, S. J., & Namdar, A. (2014). Behaviour of oil palm shell reinforced concrete beams added with kenaf Fibres. Applied Mechanics and Materials, 567, 351-355.

More, F.M.D.S. & Subramanian, S.S. (2022). Impact of fibres on the mechanical and durable behaviour of fibre-reinforced concrete. Buildings, 12(9), 1436.

Ozerkan, N. G., Ahsan, B., Mansour, S., & Iyengar, S. R. (2013). Mechanical performance and durability of treated palm fiber reinforced mortars. International Journal of Sustainable Built Environment, 2(2), 131-142.

Ramli, M., Kwan, W.H. & Abas, N.F. (2013). Strength and durability of coconut-fibre-reinforced concrete in aggressive environments. Construction and Building Materials, 38, 554-566.

Ranganathan, S., Mantena, P. R., & Nori, C. V. (2019, November). Axial loading and buckling response characteristics of pultruded hybrid glass-graphite/epoxy composite beams. In Adaptive Structures, Eighth Japan/ US Conference Proceedings (pp. 980-989). CRC Press.

SABS (2021) SANS 5865 (SABS SM 865) Concrete tests—the drilling, preparation, and testing for compressive strength of cores taken from hardened concrete for testing concrete. SABS, Pretoria, South Africa.

SABS (South African National Standard) (2021) SANS 5864: Concrete tests flexural strength of hardened concrete. SABS, Pretoria, South Africa.

Salami, B. A., Bahraq, A. A., ul Haq, M. M., Ojelade, O. A., Taiwo, R., Wahab, S., ... & Ibrahim, M. (2024). Polymerenhanced concrete: A comprehensive review of innovations and pathways for resilient and sustainable materials. Next Materials, 4, 100225. doi: https://doi.org/10.1016/j.nxmate.2024.100225.

Sgriccia, N., Hawley, M. C., & Misra, M. (2008). Characterization of natural fibre surfaces and natural fibre composites. Composites Part A: Applied Science and Manufacturing, 39(10), 1632-1637.

Smith, G., Androff, N., & Kamla, J. (1997). Moisture absorption properties of laminates used in chip packaging applications. In IPC EXPO. https://www.isola-group.com/wp-content/upl...

Thomas, B. S., Yang, J., Bahurudeen, A., Chinnu, S. N., Abdalla, J. A., Hawileh, R. A., & Hamada, H. M. (2022). Geopolymer concrete incorporating recycled aggregates: A comprehensive review. Cleaner Materials, 3, 100056.

Thomas, B. S., Yang, J., Mo, K. H., Abdalla, J. A., Hawileh, R. A., & Ariyachandra, E. (2021). Biomass ashes from agricultural wastes as supplementary cementitious materials or aggregate replacement in cement/geopolymer concrete: A comprehensive review. Journal of Building Engineering, 40, 102332.

Tran, N. P., Nguyen, T. N., & Ngo, T. D. (2022). The role of organic polymer modifiers in cementitious systems towards durable and resilient infrastructures: a systematic review. Construction and Building Materials, 360, 129562. doi: https://doi.org/10.1016/j.conbuildmat.2022.129562.

Vargas, P., Restrepo-Baena, O., & Tobón, J. I. (2017). Microstructural analysis of interfacial transition zone (ITZ) and its impact on the compressive strength of lightweight concretes. Construction and Building Materials, 137, 381-389.

Wang, W., Guo, X., Zhao, D., Liu, L., Zhang, R., & Yu, J. (2020). Water absorption and hygrothermal aging behaviour of wood-polypropylene composites. Polymers, 12(4), 782.

Wei, J., & Gencturk, B. (2018). Degradation of natural fiber in cement composites containing diatomaceous earth. Journal of Materials in Civil Engineering, 30(11), 04018282.

Xie, C., Cao, M., Khan, M., Yin, H., & Guan, J. (2021). Review on different testing methods and factors affecting fracture properties of fiber reinforced cementitious composites. Construction and Building Materials, 273, 121766.

Xie, C., Cao, M., Si, W., & Khan, M. (2020). Experimental evaluation on fiber distribution characteristics and mechanical properties of calcium carbonate whisker modified hybrid fibers reinforced cementitious composites. Construction and Building Materials, 265, 120292.

Yan, L., Chouw, N., Huang, L. & Kasal, B. (2016). Effect of alkali treatment on microstructure and mechanical properties of coir fibres, coir fibre reinforced-polymer composites and reinforced-cementitious composites. Construction and Building Materials, 112, 168-182.

Yan, L., Su, S. & Chouw, N. (2015). Microstructure, flexural properties and durability of coir fibre reinforced concrete beams externally strengthened with flax FRP composites. Composites Part B: Engineering, 80, 343-354.

Zhang, Y., Li, Y., & Zhang, Y. (2013). Cellulose synthesis in higher plants: a review. Frontiers in Plant Science, 4, p. 100. Available at: https://pmc.ncbi.nlm.nih.gov/articles/PMC3894906/ (Accessed: 29 October 2024).

Zhang, Y., Wang, Y., Zhang, Y., Liu, J., & Zhang, X. (2022). Regulation of cellulose synthesis in plants: insights from molecular and genetic studies. Molecular Plant, 15(12), 2030-2048. Available at: https://www.cell.com/molecular-plant/pdf/S1674-2052(22)00450-6.pdf (Accessed: 29 October 2024).

Notes